YMTHE, Volume *31*

Supplemental Information

Single-cell dissection of cellular and molecular features underlying mesenchymal stem cell therapy in ischemic acute kidney injury

Wenjuan Wang, Min Zhang, Xuejing Ren, Yanqi Song, Yue Xu, Kaiting Zhuang, Tuo Xiao, Xinru Guo, Siyang Wang, Quan Hong, Zhe Feng, Xiangmei Chen, and Guangyan Cai

Supplemental figures:

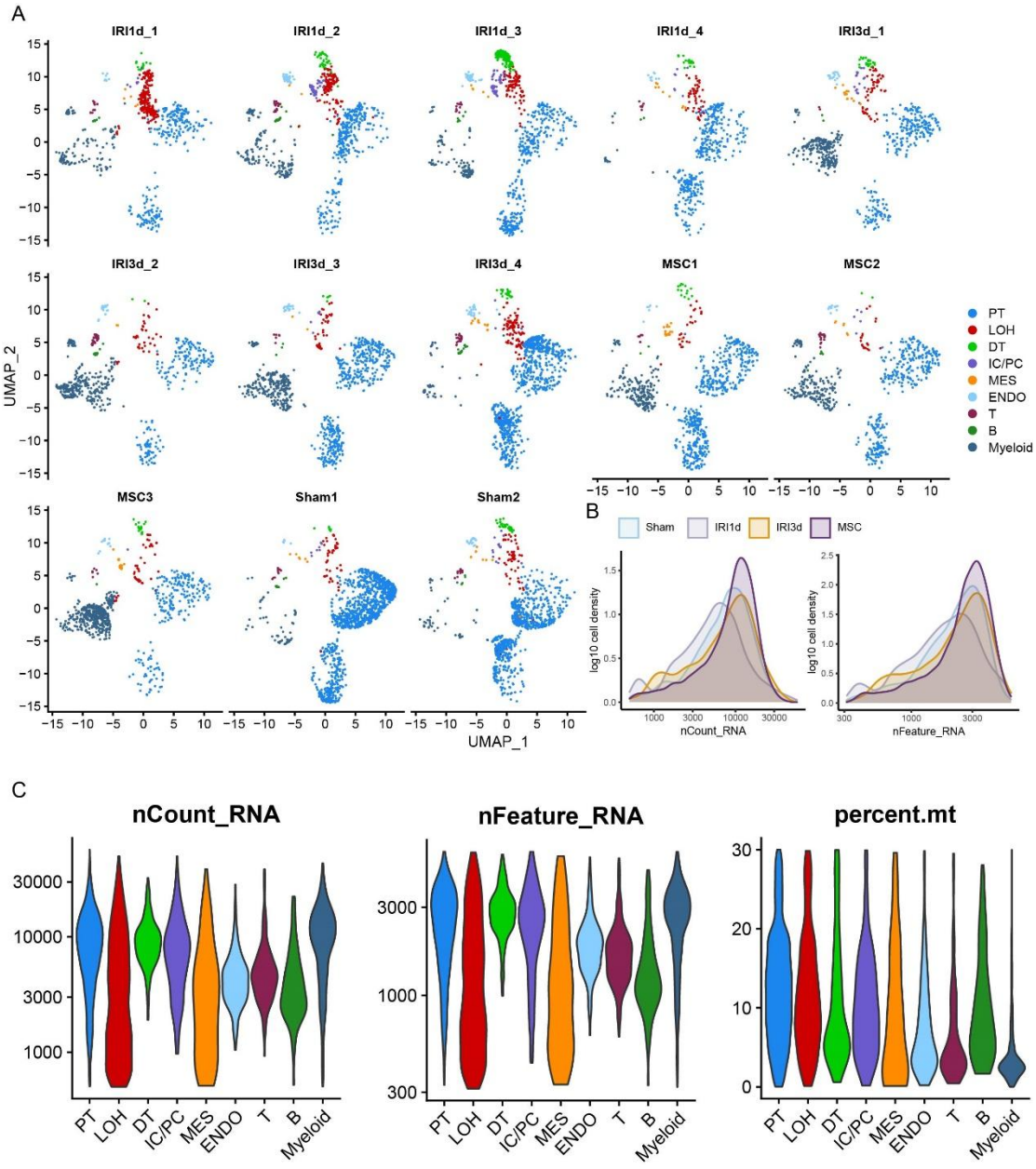

Figure S1 Data quality control and filtering criteria.

(A) The variations in distribution of cell clusters in each sample. (B) Distribution of detected gene numbers and unique molecular identifier (UMI) counts in sham, IRI-AKI, and MSC-treated kidneys. (C) The distribution of detected gene numbers and UMI counts in different cell types.

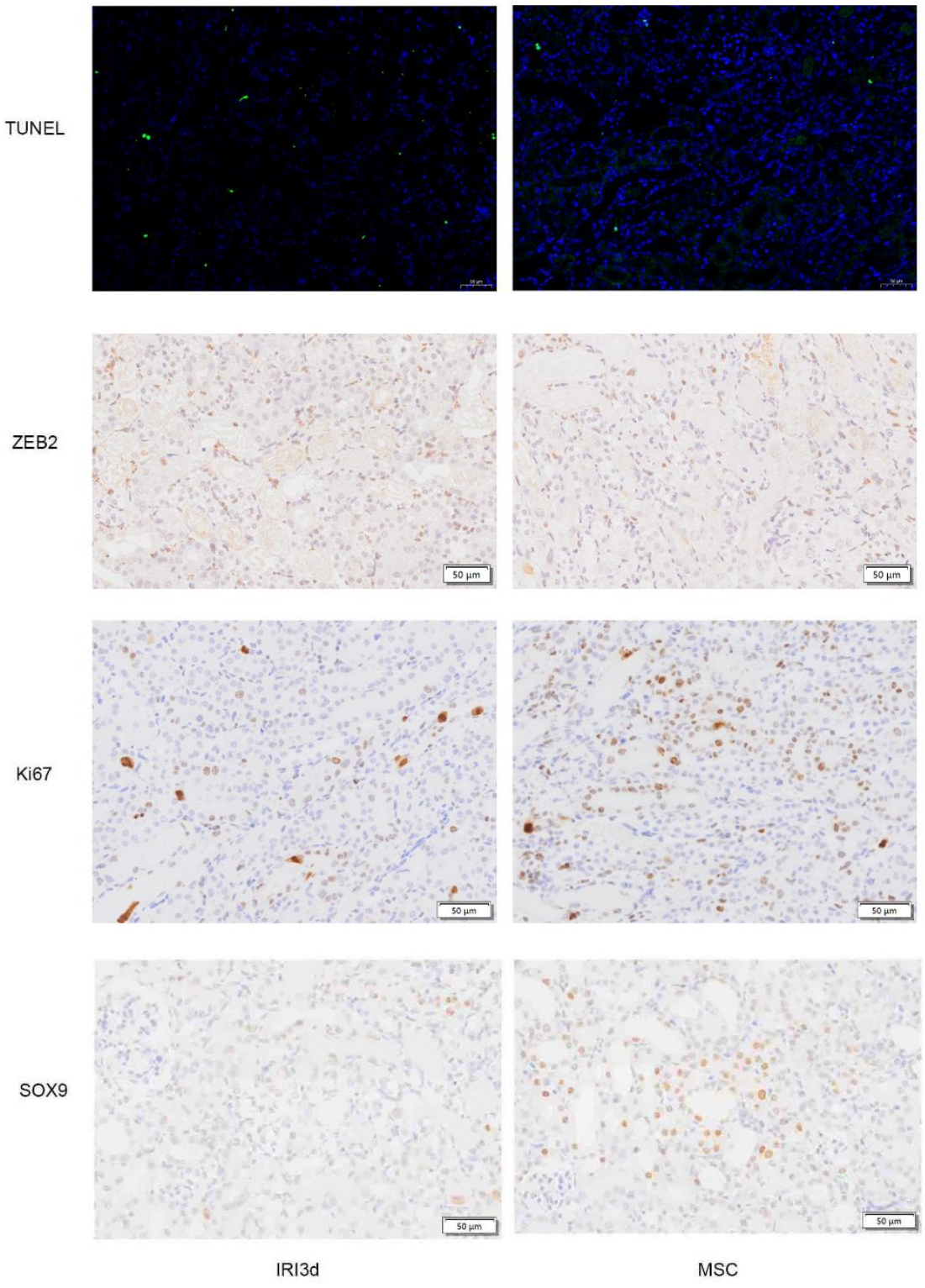

Figure S2 TUNEL staining (green) and immunohistochemical staining (brown) of ZEB2, Ki67, and SOX9 in IRI-AKI (day 3), and MSC-treated kidney tissues.

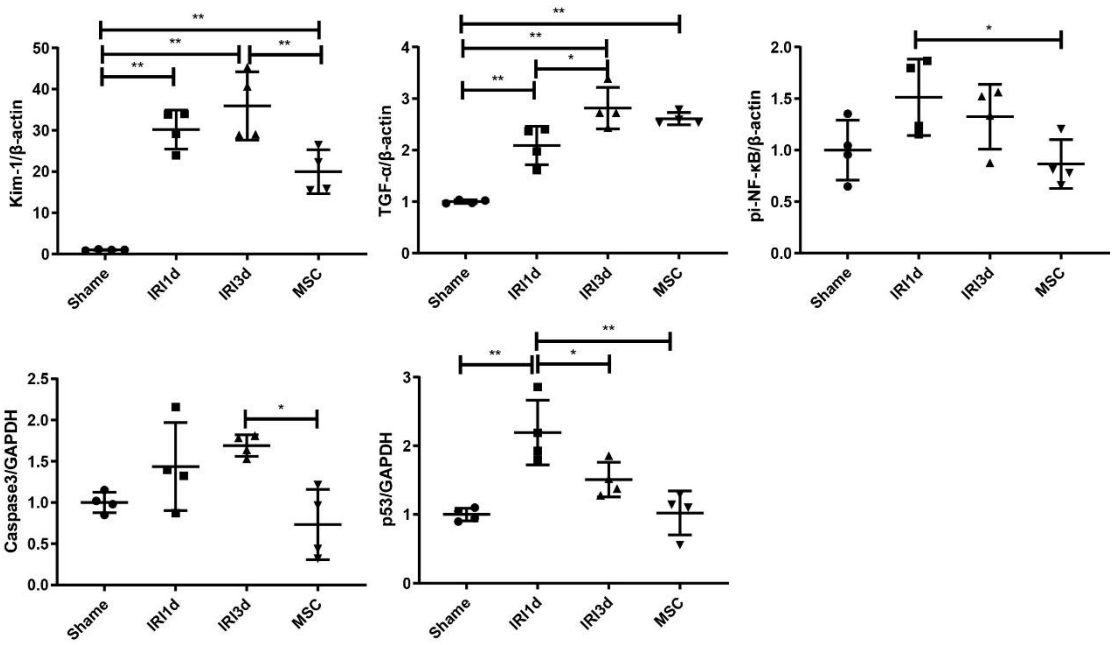

Figure S3 Semi-quantitative analysis showing the levels of KIM-1, TGF-β1, pi-NF-κB, caspase-3, and p53 proteins in sham, IRI-AKI, and MSC-treated kidney tissues (determined by western blotting). Data are expressed as mean ± SD; Student's t-test was used for comparisons of two groups; one-way ANOVA was used for comparisons of three or more groups. *$p < 0.05$, **$p < 0.01$.

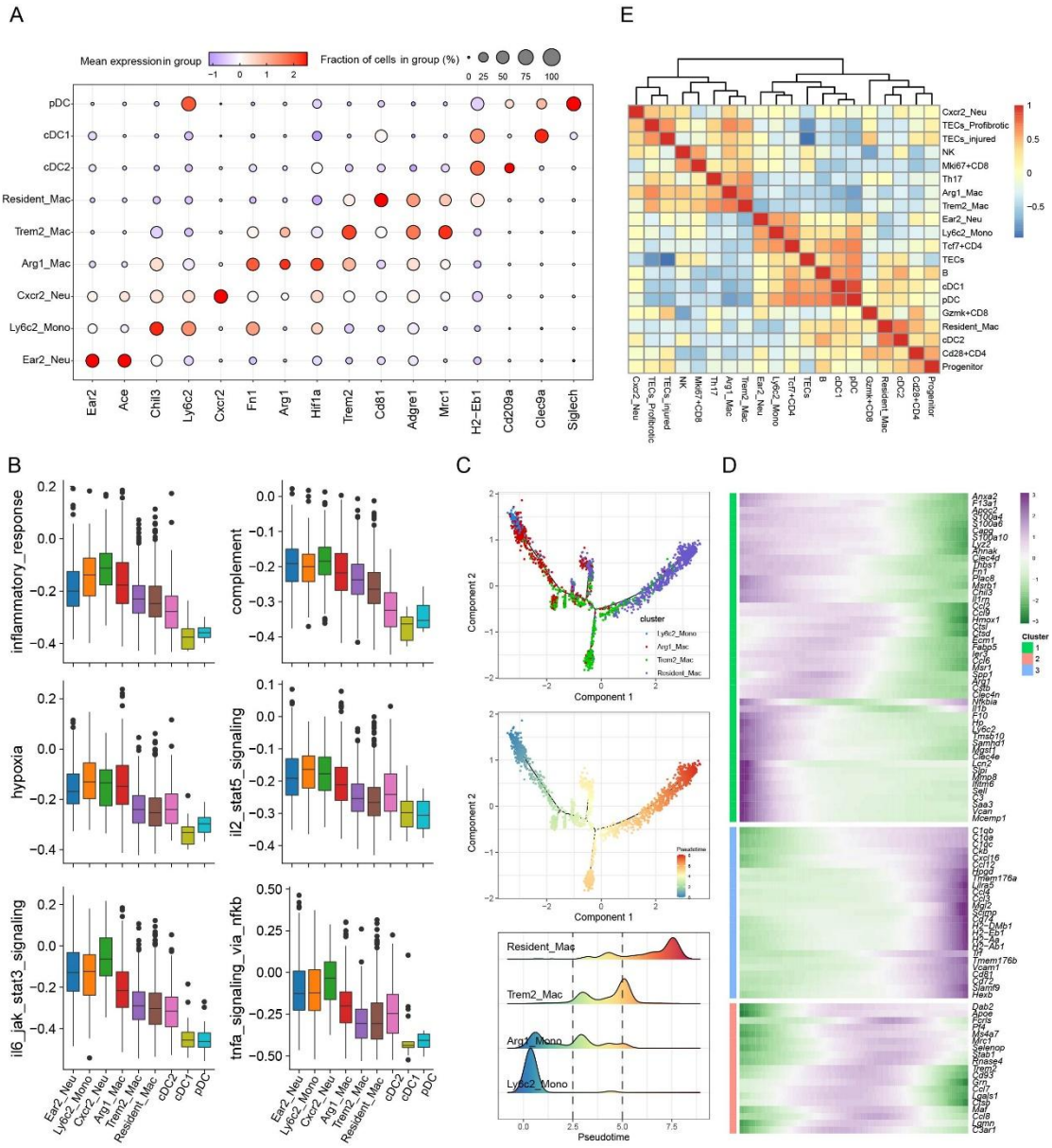

Figure S4 Cellular characteristics and pseudotime differentiation of infiltrating monocytes. (A) Dot plot showing the expression of characteristic genes in different myeloid cell types. (B) Bar plots showing the signaling pathways enriched in myeloid cell types. (C and D) Trajectory analysis showing the pseudotemporal differentiation routes of infiltrating monocytes. (E) Heatmap showing the correlations between TECs and infiltrating immune cells.

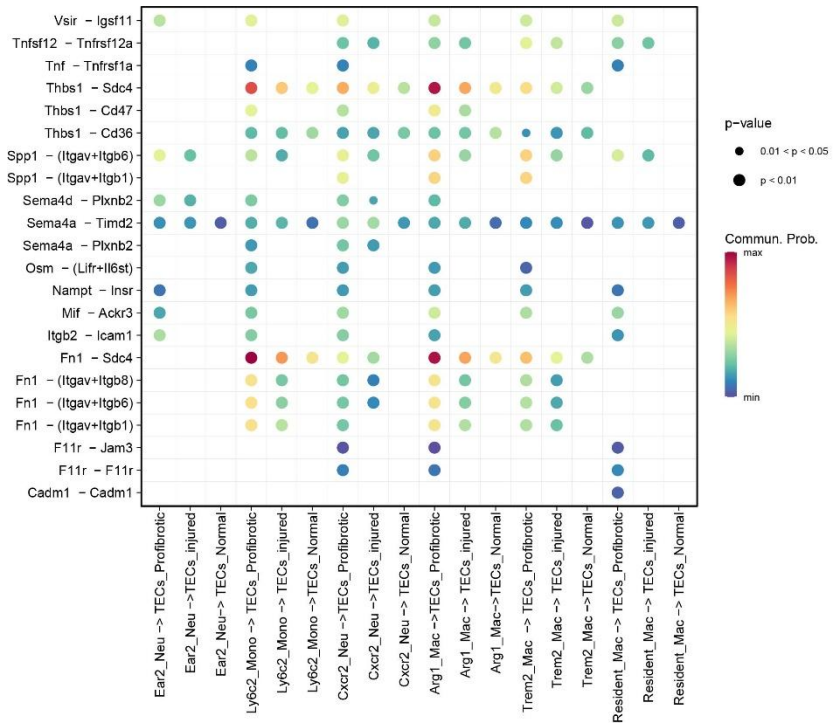

Figure S5 Dot plot showing ligand-receptor pairs for TECs and infiltrating myeloid cell subtypes.

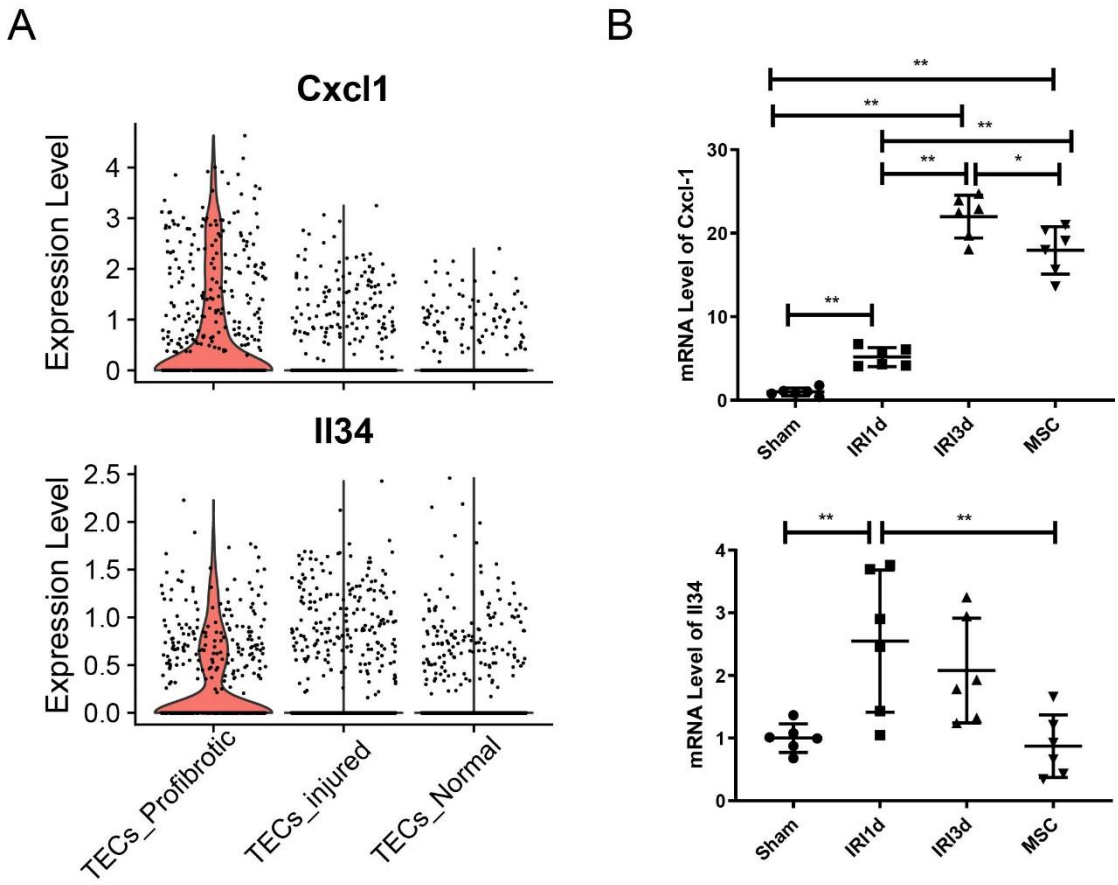

Figure S6 Detection of *Cxcl1* and *Il-34* expressed in kidney.

(A) Violin plots showing the expression of *Cxcl1* and *Il34* in TEC subtypes. (B) Results of qPCR analysis showing the mRNA levels of *Cxcl1* and *Il34* in sham, IRI-AKI, and MSC-treated kidney tissue. Data are expressed as mean ± SD; one-way ANOVA was used for comparisons of three or more groups. *p < 0.05, **p < 0.01.

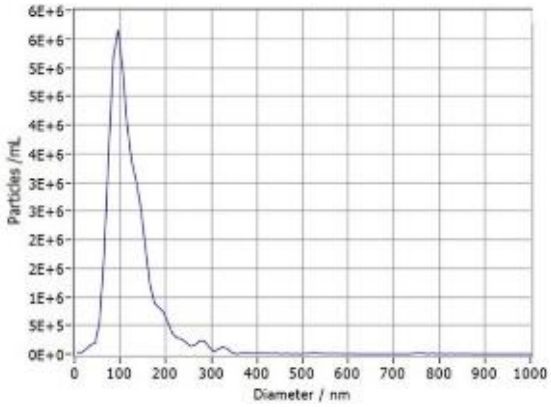

Figure S7 Nanoparticle tracking analysis (NTA) to measure the diameters of MSC-EVs.

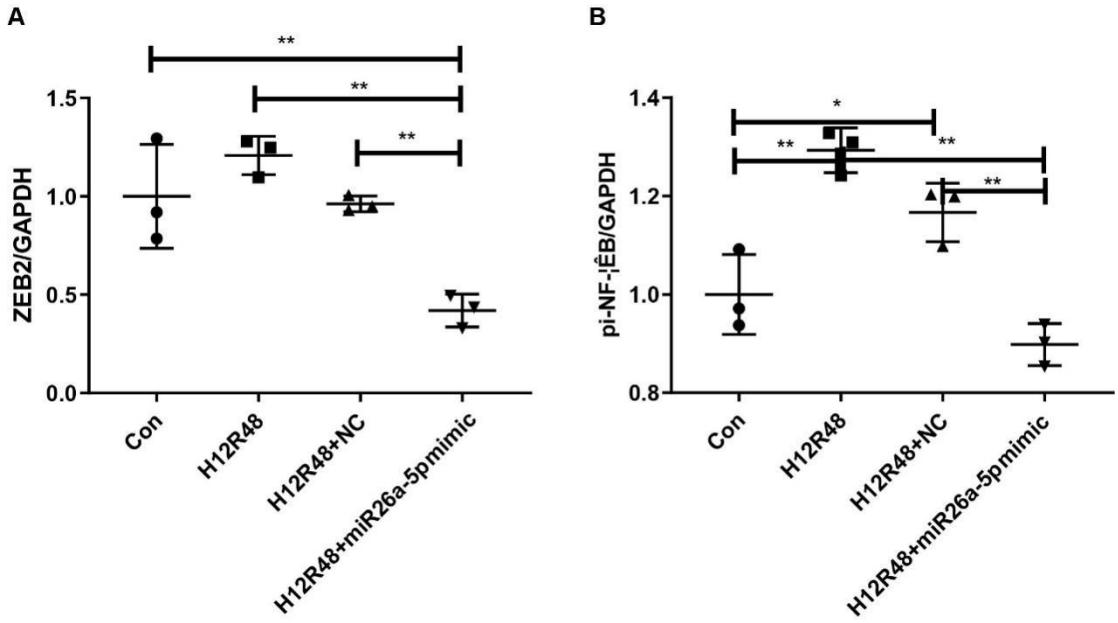

Figure S8 Semiquantitative analysis of ZEB2 (A) and pi-NF-κB (B) protein levels in HK2 cells undergoing H/R damage +/- exogenous miR-26a-5p (determined by western blotting). Data are expressed as mean ± SD; one-way ANOVA was used for comparisons of three or more groups. *p < 0.05, **p < 0.01.

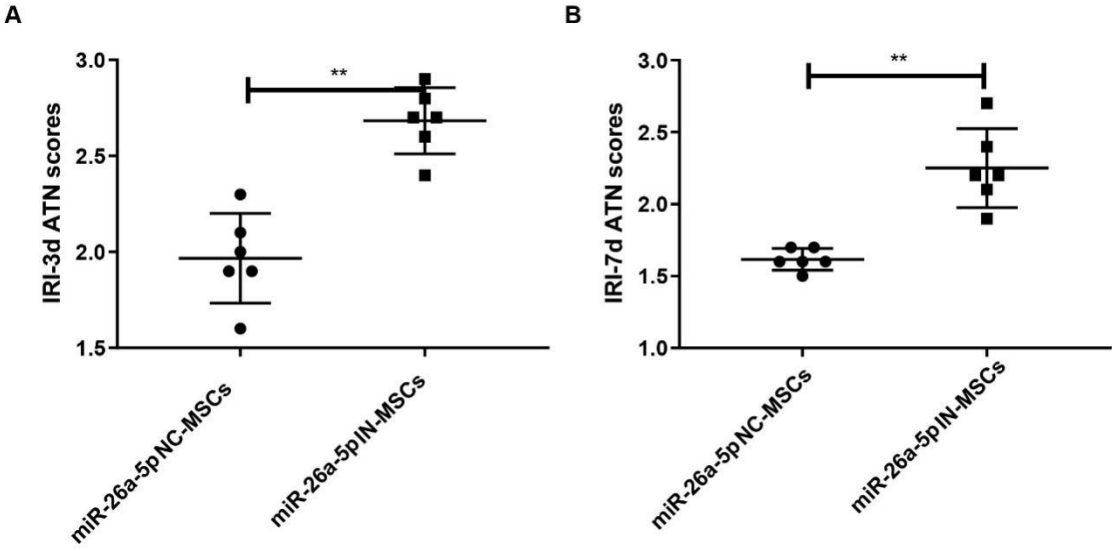

Figure S9 Effect of miR-26a-5p inhibitor in MSCs on acute tubular necrosis (ATN) scores at IRI-3 d (A) and IRI-7 d (B). Data are expressed as mean ± SD; Student's t-test was used for comparisons of two groups. **$p < 0.01$.

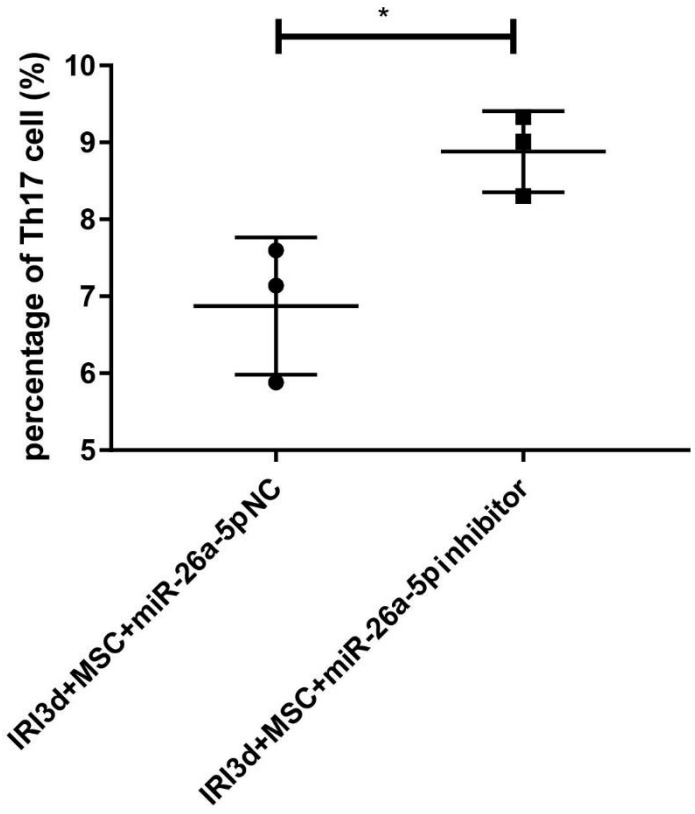

Figure S10 The quantitative analysis of Th17 cell percentage (%). Data are expressed as mean ± SD; Student's t-test was used for comparisons of two groups. *p < 0.05.

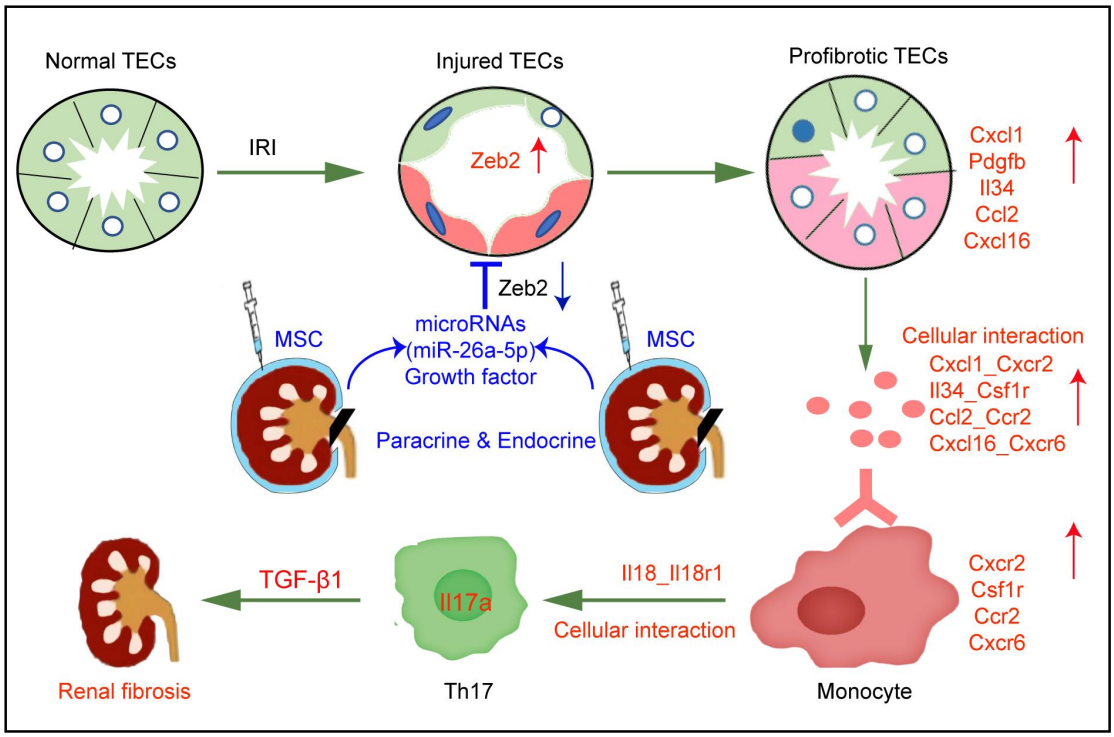

Figure S11 Summary of the role of MSCs in the regulation of kidney repair and fibrosis during AKI-CKD progression.

In AKI, abundant pro-fibrotic TECs expressing high levels of *Cxcl1*, *Il34*, and *Ccl2* mRNAs, recruit *Cxcr2*+ and *Ccr2*+ inflammatory monocytes, which in turn recruit *Il17a*+ and *Il18r1*+ Th17 cells, leading to TGF-β1 secretion and renal fibrosis; MSC-derived miR-26a-5p suppresses *Zeb2* expression, decreasing the proportion of pro-fibrotic TECs and Th17 cells and inhibiting renal fibrosis.